

04,10,12

## Simulating 2D-Diffraction Patterns of Model Gallium Arsenide Whisker Crystals

© M.D. Sharkov, N.D. Prasolov, A.A. Levin, P.N. Brunkov

Ioffe Institute,  
St. Petersburg, Russia  
E-mail: mischar@mail.ru

Received October 4, 2022

Revised October 4, 2022

Accepted October 11, 2022

A set of GaAs whisker crystallites in the shape of hexagonal prism with the axis along the [111] direction have been modeled as well as constructions consisting of such prisms. For these model samples XRD patterns have been calculated. Basing on the calculated XRD pattern analysis, a fitting configuration of prismatic fragments has been built for an atomic array obtained with the help of applying molecular dynamics techniques to the initial model prismatic GaAs crystallite.

**Keywords:** whiskers, XRD pattern simulation, A<sup>III</sup>B<sup>V</sup> semiconductors, gallium arsenide.

DOI: 10.21883/PSS.2023.01.54981.493

### 1. Introduction

Nanoscale objects (clusters, domains, crystallites) may exhibit different physicochemical properties than the same materials in a macroscopic volume. In particular, crystallites can differ significantly from bulk material already at the level of atomic structure, which can be reflected, for example, in X-ray diffraction patterns. Hence the importance of the tasks associated with the direct calculation of diffraction patterns from nanostructures, in incl. crystallites. From the comparison of the model pattern of X-ray diffractometry (XRD) with experimental data, conclusions can be drawn about the structural features of the crystallites in the sample under study.

GaAs gallium arsenide is a straight-band semiconductor with the band gap width 1.4 eV and has a cubic lattice with a sphalerite structure (space group  $F\bar{4}3m$  (216)) and a lattice parameter of 5.653 Å [1] (map 01-089-2706 in the powder diffraction database PDF-2 [2]). Semiconductor heterostructures based on GaAs and other elements of the 3 and 5 groups of the periodic table [3] are widespread. Structures based on the application of GaAs together with elements of other groups [4,5] are actively investigated. Gallium arsenide can be obtained both in the form of thin films and in bulk form [6], which makes it possible to research and practical operation of various crystallographic surfaces of GaAs, incl., the most densely packed plane (111). Of particular interest are filamentous crystals (whiskers) GaAs [7,8], which, due to their quasi-one-dimensional (quasi-1D) geometry, differ significantly in properties from both bulk material and thin films/layers.

The calculation of the structural factor of X-ray scattering by materials underlies such methods of diffractogram analysis as the Rietveld methods [9,10], Pawley's technique [11] and Le Bail's one [12]. In the listed methods of modeling

XRD patterns, only the characteristics of the elementary cells of the crystal components of the object from which the model is constructed XRD [13,14] are considered. However, there are also such works in which the XRD curves from model structures consisting of hundreds [15] and thousands [16,17] atoms are directly calculated, and in the work [18] diffractograms from a model crystallite of about 400 thousand Pd atoms are constructed.

In this paper, modeling and subsequent analysis of two-dimensional (2D) XRD patterns from GaAs model whiskers containing about a million atoms are carried out. In this case, the intensity of the XRD is calculated through the total structural factor of X-ray scattering over the entire given array of whisker atoms.

### 2. Methods

GaAs crystallite modeling was carried out by molecular dynamics methods using a package called Large-Scale Atomic/Molecular Massively Parallel Simulator (LAMMPS) [19,20]. In the LAMMPS program, a crystal lattice is built on the basis of an elementary cell, information about which can be either taken from a ready-made template or entered manually. In the simulation process, temperature is taken into account as an additional factor that can affect the actual arrangement of atoms in the crystallite.

The calculation of the XRD data was carried out using standard procedures [21–24]. A modeling method was used based on the description of the intensity of X-ray scattering by matter through atomic and structural factors [21,22]:

$$I \propto \Phi(\theta)A(\theta)D(\theta) \left| \sum_j f_j(q) \exp(i\mathbf{q}\mathbf{r}_j) \right|^2. \quad (1)$$

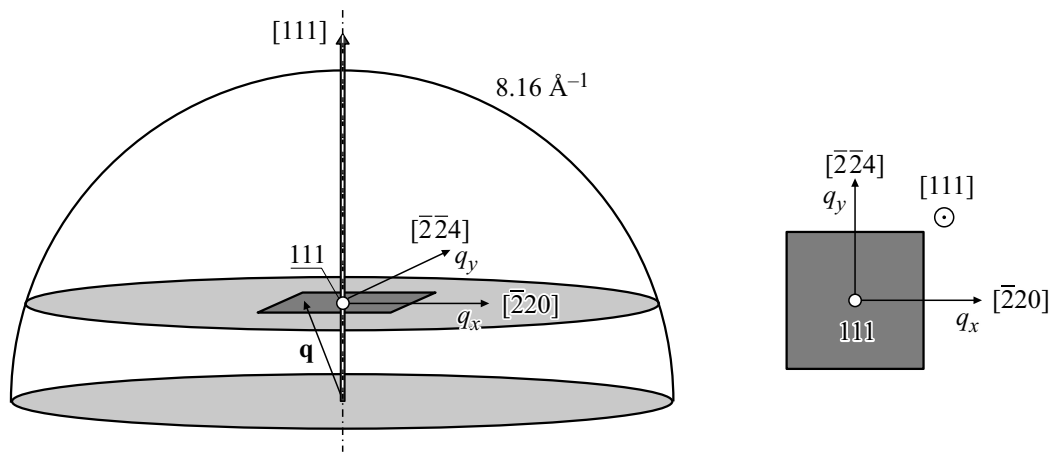


**Figure 1.** The area of construction of model diffraction patterns. The following are marked in the figure: the node of the reciprocal lattice 111 (light circle); the boundary of the XRD data registration area for  $\text{Cu } K_{\alpha 1}$ -radiation (large semicircle); planes (111) (light gray ellipses); directions  $[\bar{1}10]$  and  $[\bar{1}\bar{1}2]$ , which correspond to the components of the wave vector  $q_x$  and  $q_y$ . The range of the scattering wave vector  $\mathbf{q}$  corresponding to the area of diffractograms is highlighted in a darker tone.

Here  $2\theta$  is the X-ray diffraction angle;  $\Phi(\theta) = (1 + \cos^2 2\theta)/(\sin^2 \theta \cos \theta)$  is the coefficient obtained by theoretical consideration of the X-ray photon scattering problem [23] and called the Lorentz polarization factor of X-ray radiation;  $A(\theta) = \exp(-2\mu t / \sin \theta)$  is the value characterizing the attenuation of the beam intensity when it penetrates into the sample to a depth of  $t$  (taking into account the output of reflected photons) in accordance with the Bouguer–Lambert–Beer law [22,25];  $\mu$  is the absorption coefficient of the material;  $D(\theta)$  is the Debye–Waller factor caused by thermal vibrations of atoms of the model material;  $f_j(q)$  is the scattering amplitude of X-ray photons by the  $j$ -th atom, the photons having a scattering wave vector  $\mathbf{q}$  (which is modulo  $4\pi \sin \theta / \lambda$ ). In the first approximation, it is assumed that the value of  $A(\theta)D(\theta)$  is close to unity and does not significantly affect the diffraction pattern.

Atomic scattering factors are calculated based on the model described in the literature [24]:

$$f_j(q) = \sum_k a_k \exp(-c_k q^2) + \text{const}, \quad (2)$$

moreover, the sets of model parameters ( $a_k$ ,  $c_k$  and const), individual for each atom and/or ion, are given in the same reference [24]. The scattering vectors at which this model ceases to correspond to experimental data correspond to values  $q$  (modulo) greater than or of the order-of-magnitude of  $25 \text{ \AA}^{-1}$  (which can be experimentally observed on diffractograms only with radiation with a beam energy of 25 keV and higher).

### 3. Results

A GaAs crystallite whisker was modeled in the form of a hexagonal prism of regular cross-section with a diameter (double the length of the rib) of a hexagonal base 15

and height 150 nm. The axis of the prism corresponds to the crystallographic direction [111], the faces are parallel to the planes  $(01\bar{1})$ ,  $(\bar{1}01)$  and  $(1\bar{1}0)$ . The edges of the prism base are oriented in the directions  $[\bar{1}\bar{1}2]$ ,  $[\bar{1}2\bar{1}]$ ,  $[2\bar{1}\bar{1}]$ . The model crystallite contains about  $9.71 \cdot 10^5$  atoms and has  $C_{3v}$  symmetry. During modeling, it was assumed that the crystallite was initially located in a vacuum and did not contain any point or dimensional defects, and its surface was not subject to reconstruction.

In addition to the initial state of the crystallite, its appearance in space was modeled at time intervals up to 32 ps with 20 fs increments (starting from the initial state) based on molecular dynamics methods using the LAMMPS program. During the simulation, it was assumed that the temperature of the crystallite is constant and 300 K.

For all simulated GaAs crystallites, the XRD data were calculated in accordance with the methodology described above. Models of diffraction patterns are constructed for radiation with photon energy corresponding to  $\text{Cu } K_{\alpha 1}$ -radiation (wavelength 1.5406 Å). The data region in which the diffraction patterns are constructed is a plane parallel to the crystallographic plane (111) in the GaAs lattice and passing through the node of the reciprocal GaAs lattice 111 (see Fig. 1). In all cases, the plane (111) and the node 111 for the GaAs lattice in the initial state of the crystallite were considered. Here and further,  $q_0$  denotes the magnitude of the wave vector, which corresponds to the modulus of the node scattering vector 111 for GaAs (approximately  $1.925 \text{ \AA}^{-1}$ ).

Fig. 2 shows a model of the scattering pattern obtained from a GaAs crystallite constructed as a regular set of atoms and representing the initial structure, to which molecular dynamics methods were then applied using the LAMMPS package. In Fig. 3, *a* — the same for the same crystallite at the time of molecular dynamics simulation 8 ps, in Fig. 3, *b, c, d* — through 16, 24 and 32 ps,

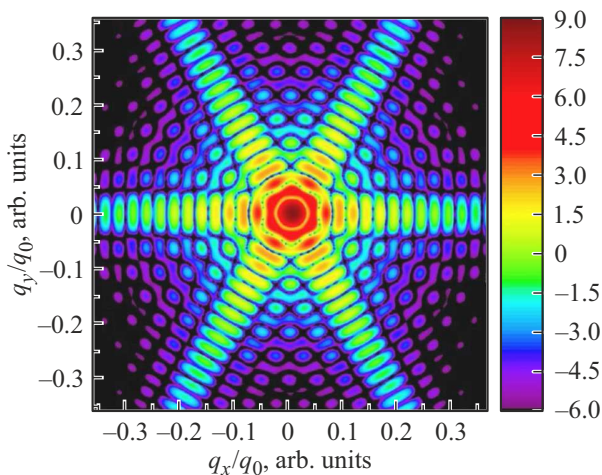


**Figure 2.** The calculated 2D-XRD pattern from the GaAs model crystallite considered in this paper in the form of a hexagonal prism with a height of 150 nm and a base edge length of 7.5 nm in the initial state (Cu  $K_{\alpha 1}$ -radiation). The value  $q_0 = 1.925 \text{ \AA}^{-1}$  corresponds to the length of the wave vector of node 111 of the reciprocal GaAs lattice.

respectively. The directions  $q_x$  and  $q_y$  in all the picture models correspond to the crystallographic directions  $[\bar{1}10]$  and  $[\bar{1}\bar{1}2]$ , respectively (for the lattice of the crystallite in the initial state).

The general view of the XRD pattern in the vicinity of the reciprocal lattice node 111 at the initial moment of time is associated with the symmetry of the lattice (space group  $F\bar{4}3m$  (216)) and with the shape of the crystallite. The whisker configuration determines the directions in which the most intense satellite peaks are located. In this case — for a hexagonal prism with axis  $[111]$  and side faces along the planes  $(01\bar{1})$ ,  $(\bar{1}01)$  and  $(1\bar{1}0)$  — the most intense satellite peaks around the reciprocal lattice node 111 are observed in the directions  $[01\bar{1}]$ ,  $[\bar{1}01]$  and  $[1\bar{1}0]$ , perpendicular to the planes of the side faces.

Visual observation of the behavior of the simulated crystallite in real space shows that during the simulation of molecular dynamics in the time interval 0–32 ps, its structure changes significantly, forming, in fact, several separate crystalline phases. Several areas of high intensity are observed, deviated from the center of the picture by

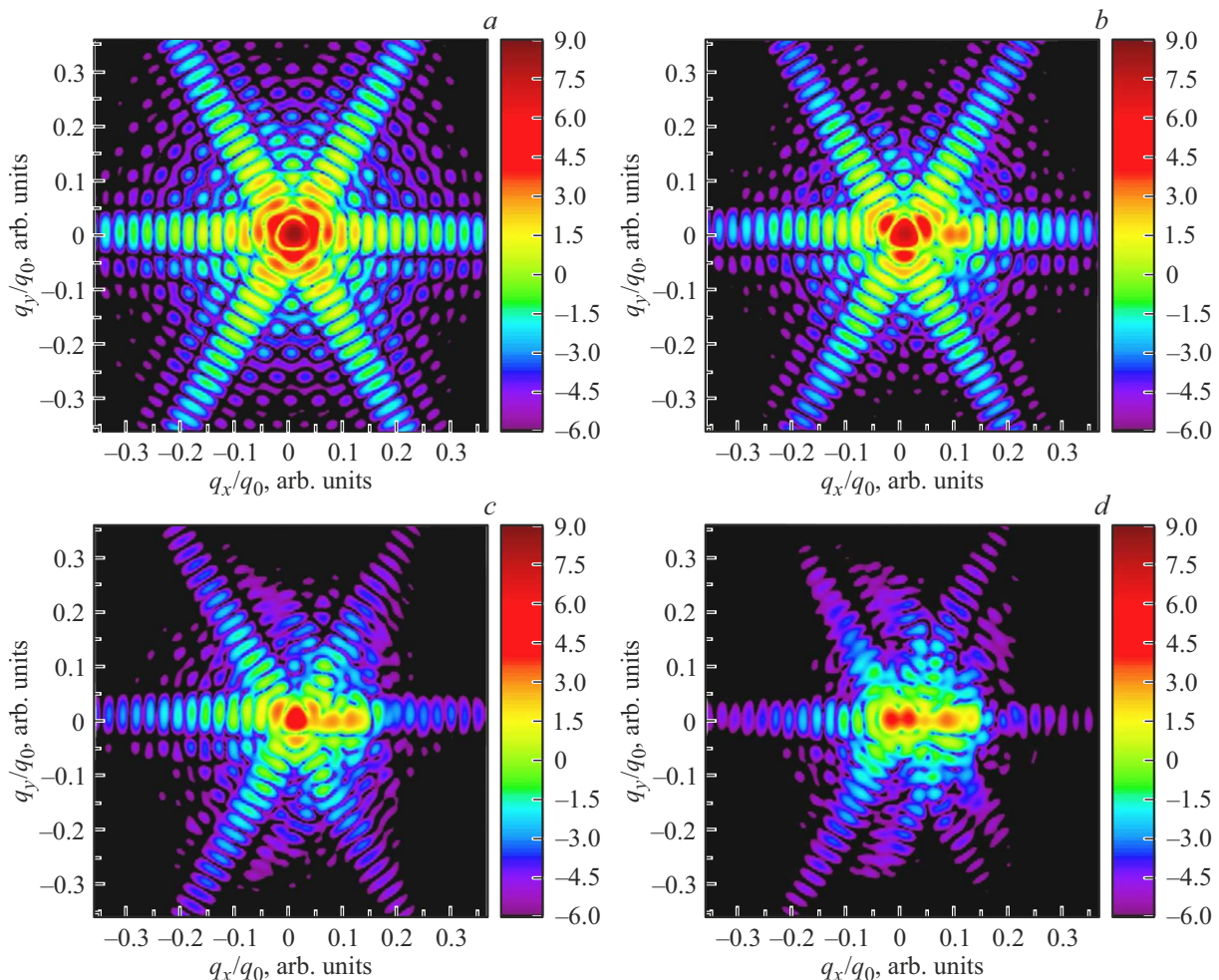


**Figure 3.** Calculated 2D-XRD patterns from the GaAs model crystallite considered in this paper in the form of a hexagonal prism with a height of 150 nm and a base edge length of 7.5 nm for Cu  $K_{\alpha}$ -radiation in the calculated molecular dynamics simulation time points: (a) 8 ps, (b) 16 ps, (c) 24 ps, (d) 32 ps. The value  $q_0 = 1.925 \text{ \AA}^{-1}$  corresponds to the length of the wave vector of node 111 of the reciprocal GaAs lattice.

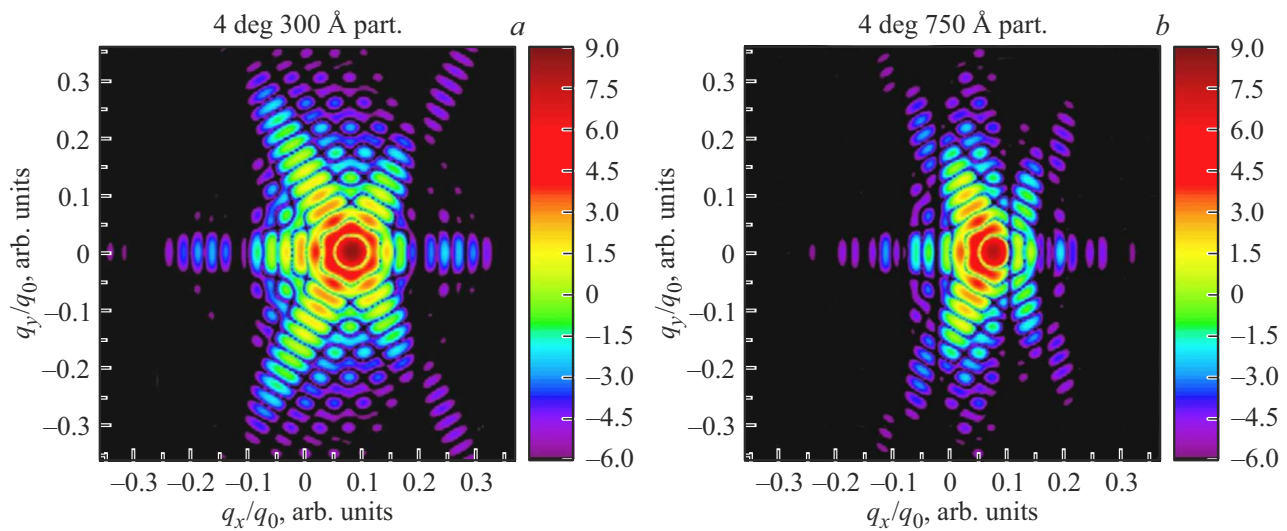


**Figure 4.** Diffraction patterns (Cu  $K_{\alpha 1}$ -radiation) from model crystallites in the form of hexagonal prisms rotated in the direction of  $[1\bar{1}0]$  by  $4^\circ$  relative to the initial orientation, at the height of the prisms 30 nm (a) and 75 nm (b) and the length of the base edge 7.5 nm. The pictures center corresponds to the node of the wave vector of the node 111 of the reciprocal GaAs lattice in the initial (non-rotated) position. The value  $q_0 = 1.925 \text{ \AA}^{-1}$  corresponds to the length of the wave vector of node 111 of the reciprocal GaAs lattice.

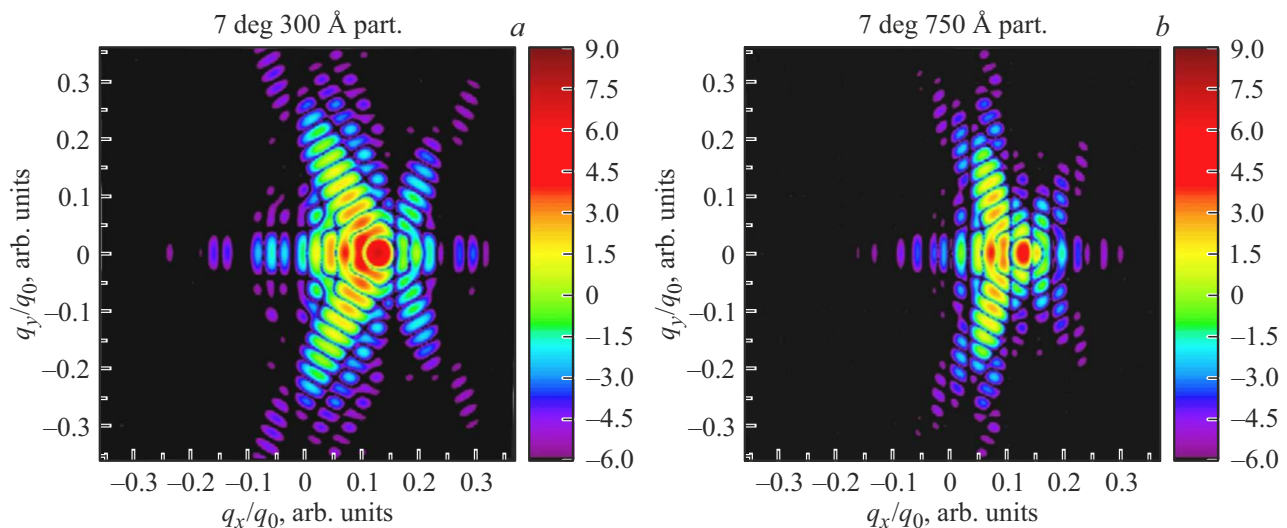


**Figure 5.** Diffraction patterns (Cu  $K_{\alpha 1}$ -radiation) from model crystallites in the form of hexagonal prisms rotated in the direction of  $[1\bar{1}0]$  by  $7^\circ$  relative to the initial orientation, at a height of 30 nm (a) and 75 nm (b) and the length of the base edge 7.5 nm. The pictures center corresponds to the node of the wave vector of the node 111 of the inverse GaAs lattice in the initial (non-inverted) position. The value  $q_0 = 1.925 \text{ \AA}^{-1}$  corresponds to the length of the wave vector of node 111 of the inverse GaAs lattice.

angles up to  $7^\circ$  in the direction of the direction  $[1\bar{1}0]$  of the reciprocal lattice of the original crystallite matrix. Hence, it can be assumed that the model structure contains separate domains that retain the shape of a hexagonal prism as a whole, but are rotated relative to the initial orientation of the model crystallite by small angles (up to  $7^\circ$ ) in the direction of  $[1\bar{1}0]$  of the original lattice (a also, probably in the opposite direction  $[1\bar{1}0]$  at angles not more than  $1^\circ$ ).

The following figures show the results of modeling diffraction patterns from GaAs model crystallites, differing in length along the prism axis (30 and 75 nm) and deviation

angle (4 and  $7^\circ$ ), as well as structures composed of rotated and non-rotated crystallite.

Fig. 4, a, b shows diffraction patterns constructed for model crystallites of lengths 30 and 75 nm rotated by angle  $4^\circ$  in the direction  $[1\bar{1}0]$  (around the axis in direction  $[\bar{1}\bar{1}2]$ ) relative to the initial orientation of the crystallite. Fig. 5, a, b shows similar diffraction patterns for the rotation angle  $7^\circ$ .

For diffraction patterns calculated from rotated model crystallites, there is an offset of the diffraction structure by approximately the angle of rotation with the preservation

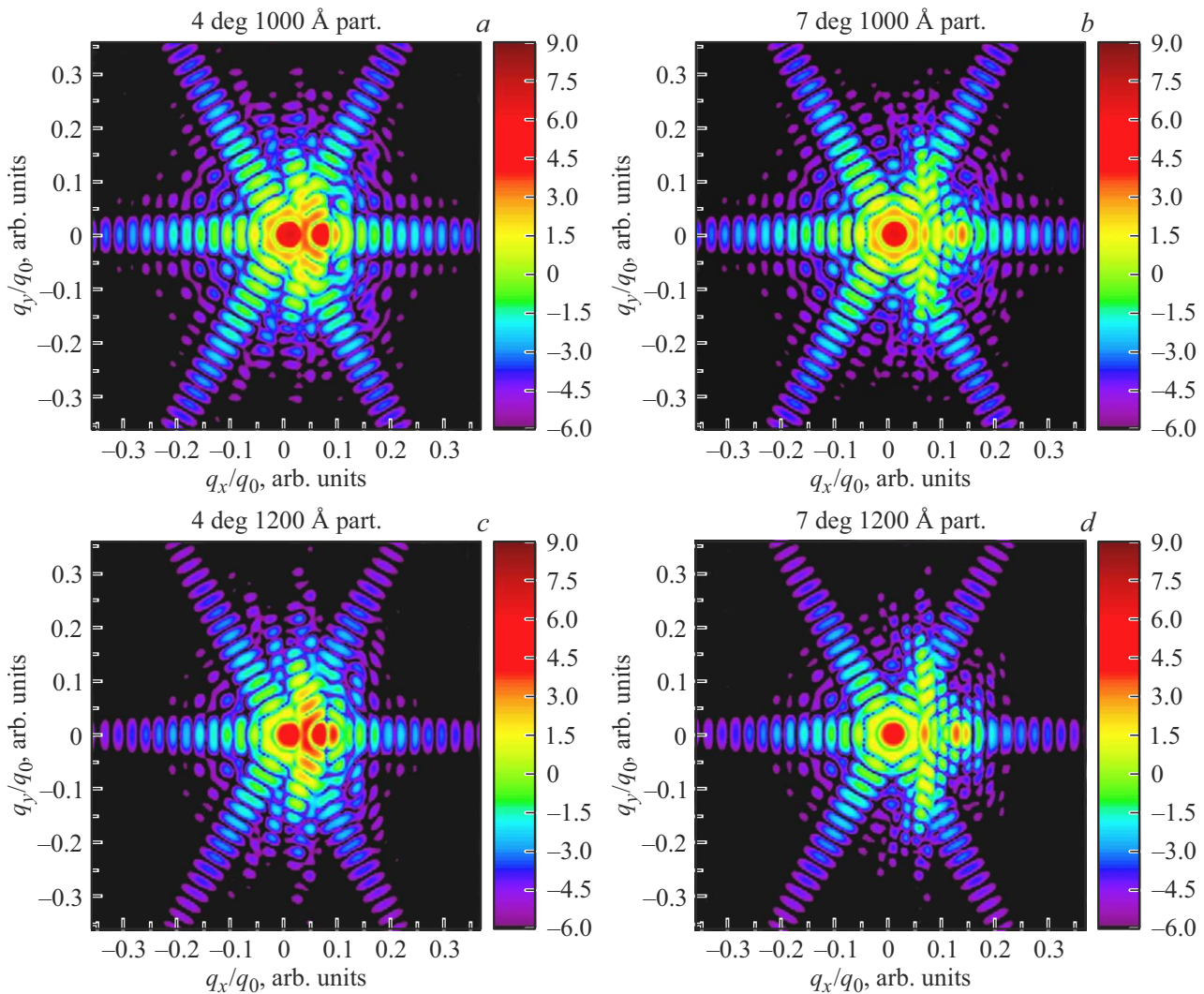


**Figure 6.** Diffraction patterns ( $\text{Cu}K_{\alpha 1}$ -radiation) from model samples consisting of two fragments in the form of hexagonal prisms: unturned and rotated in the direction of  $[1\bar{1}0]$ . The lengths (heights of the prisms) of the non-rotated part, the rotated part and the angle of rotation are respectively: 50, 100 nm,  $4^\circ$  (a); 50, 100 nm,  $7^\circ$  (b); 30, 120 nm,  $4^\circ$  (c); 30, 120 nm,  $7^\circ$  (d). The base edge length in all cases is 7.5 nm. The pictures center corresponds to the node of the wave vector of the node 111 of the reciprocal GaAs lattice in the initial (non-rotated) position. The value  $q_0 = 1.925 \text{ \AA}^{-1}$  corresponds to the length of the wave vector of node 111 of the reciprocal GaAs lattice.

(in whole) of the appearance of a six-pointed star (symmetry  $C_{6v}$ ) in the central part of the star-shaped figure and its immediate surroundings. At the same time, the plane in which the diffraction patterns are constructed no longer corresponds to the plane with the nodes of the rotated lattice and is deviated from the latter by the angle of rotation of the model crystallite. For this reason, the center of the star-shaped figure observed in the paintings is shifted relative to the node 111 of the reciprocal lattice of the rotated crystallite by the value  $q_0(1/\cos\alpha - 1)$  (where  $\alpha$  — the angle of rotation of the crystallite) in the direction of the new axis of the crystallite. A similar pattern is observed in Fig. 3, d for the diffractogram calculated from the structure obtained from the initial crystallite using molecular dynamics modeling processes during the model time 32 ps.

Due to the rotation of the crystallographic plane (111), the scattering intensity in the region of the star-shaped figure is expected to decrease. With an increase in the angle of rotation, the central part of the star-shaped figure deviates more and more from the node 111 of the reciprocal lattice of the rotated crystallite, which is why, with increasing length of the rotated crystallite, the intensity of the diffraction pattern in the central part of the star-shaped figure decreases. Calculations show that with the normalization used in the construction of diffraction patterns in the framework of this paper, the dependence of the intensity in the center of the star-shaped figure on the length of the rotated model crystallite with small deviations from the reciprocal lattice node is proportional to a value approximately equal to  $\exp(-l^2/L_0^2)$ , where  $l$  is the length of the rotated fragment,

Estimates of rotation angles and lengths of hypothetical composite fragments (heights of composite fragments in the form of hexagonal prisms with the length of the base edge 7.5 nm) of a GaAs crystallite formed according to the results of modeling molecular dynamics processes at a given simulation time 32 ps

| Position of the maximum, ° | Intensity, arb. units | Fragment Length (evaluation), nm |
|----------------------------|-----------------------|----------------------------------|
| -1.4                       | 66.5                  | 15.6                             |
| 0.4                        | 63.6                  | 15.2                             |
| 2.2                        | 11.3                  | 6.4                              |
| 4.4                        | 26.9                  | 10.0                             |
| 7.0                        | 6.7                   | 52.4                             |

and  $L_0$  is some characteristic spatial size. For a GaAs whisker oriented in the direction of  $[111]$ , with a deviation of  $7^\circ$  from node 111, the value of  $L_0$  is about 24 nm.

As mentioned above, the plane in which the diffraction patterns are constructed in Fig. 4 and 5, rotated relative to the plane with the nodes of the reciprocal lattice by the angle of rotation of the crystallite. Therefore, in the diffraction patterns shown in Fig. 4 and 5, there are vertical bands of reduced intensity. These bands represent intersections of the area of diffraction pattern construction with regions of reduced intensity formed around planes perpendicular to the axis of the prism. Accordingly, the distance between the low intensity bands is determined by the size of the crystallite in the direction along the axis of the prism.

Fig. 6 shows diffraction patterns constructed for model samples consisting of two homogeneous fragments, one of which is part of the original model crystallite, and the second is rotated relative to the first in the direction of  $[1\bar{1}0]$ . The pictures in Fig. 6 are obtained for the rotation angles of the second fragment 4 and  $7^\circ$ , when the lengths of the non-rotated and rotated parts are 50 and 100 nm in one case, and — 30 and 120 nm in the other accordingly.

The diffraction patterns shown in Fig. 6 contain characteristic components from both fragments of the model sample. The central section of the star-shaped figure corresponding to the non rotated fragment generally retains its shape and symmetry  $C_{6v}$ , but its intensity is significantly reduced compared to the original model crystallite (proportional to the square of the extent of the non rotated part). The component of the diffraction pattern corresponding to the rotated fragment retains the main characteristic features, in particular, the bands of reduced intensity. However, due to the fact that the diffracting object is composite, the contrast of these bands is significantly reduced compared to the pictures obtained exclusively from rotated fragments.

In general, the diffraction pattern obtained from a crystallite subjected to modeling of molecular dynamics processes for 32 ps, looks similar to the pattern from a set of individual crystallites rotated at different angles mainly in the

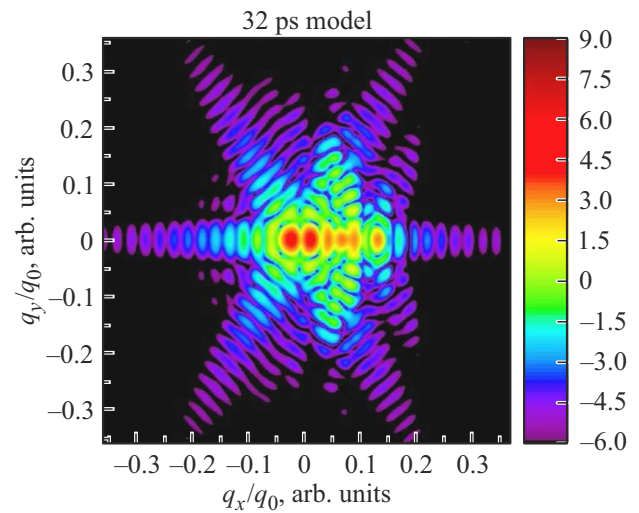


**Figure 7.** Diffraction pattern ( $\text{Cu } K_{\alpha 1}$ -radiation) from a model structure composed of homogeneous GaAs fragments in the form of hexagonal prisms with the same cross-section as the original crystallite, and the length (height of the prisms) and rotation angles corresponding to the data from the table.

direction of  $[1\bar{1}0]$ . The table shows the angles corresponding to local maxima and estimates of the length of fragments that each of them would have to have in order to give an intensity corresponding to the corresponding maximum in the diffraction pattern in Fig. 3, *d*.

Fig. 7 shows a model of the diffraction pattern obtained from a model structure composed of homogeneous GaAs fragments with the same cross-section as the original crystallite, and the length and rotation angles corresponding to the data from the table.

There are differences between the pictures shown in Fig. 3, *d* and Fig. 7, in t. h. less pronounced vertical lines of intensity attenuation in Fig. 3, *d*. On Fig. 7 these lead to the appearance of another local maximum in the direction of  $[1\bar{1}0]$  (i.e. the horizontal axis) from the center of the picture. This circumstance may indicate both the shorter length of the composite fragments and their distortion in the direction of  $[1\bar{1}0]$  local lattices of fragments. In addition, when constructing the model picture in Fig. 7, the part of the whisker not included in the hypothetical fragments listed in the table (about a third of the whisker in total) was not taken into account. Nevertheless, there is a significant similarity between the diffraction patterns in Fig. 3, *d* and Fig. 7, especially in the vicinity of spots of maximum intensity in the central part of the diffraction patterns.

## 4. Conclusion

A technique has been developed for modeling XRD patterns from model atomic matrices based on the calculation of the total scattering amplitude of monochromatic X-ray radiation from all atoms of the matrix.

Using the developed method, the XRD patterns from a number of GaAs model samples in the form of a hexagonal prism with an axis oriented along the direction of [111], as well as from model samples composed of prismatic fragments-GaAs crystallites rotated relative to each other at small angles (up to  $7^\circ$ ), were simulated. In addition, XRD patterns from model samples were calculated, representing the results of modeling molecular dynamics processes at a temperature of 300 K for the initial sample that was a prismatic GaAs crystallite with axis oriented along the direction [111], during calculated time intervals up to 32 ps in time increments scale 20 fs. The size and rotation angles of the prismatic homogeneous fragments of the structure obtained by modeling the processes of molecular dynamics at a temperature of 300 K for the initial sample during the calculated time interval of 32 ps are estimated.

### Funding

This was performed under State assignment No. 0040-2019-0009.

### Acknowledgments

The authors would like to thank S.A. Rukolaine and A.G. Panfilov (FTI named after A.F. Ioffe) for fruitful cooperation.

### Conflict of interest

The authors declare that they have no conflict of interest.

### References

- [1] G.V. Ozolins, G.K. Averkieva, A.F. Ievins, N.A. Goryunova. *Kristallografiya* **7**, 850 (1962). (in Russian).
- [2] International Centre for Diffraction Data (ICDD). Powder Diffraction File-2 Release 2014. ICDD: Newton Square, PA, USA (2014).
- [3] Zh.I. Alferov, V.M. Andreev, V.D. Rumyantsev. *Springer Ser. Opt. Sci.* **130**, 25 (2007).
- [4] S.S. Khludkov, O.P. Tolbanov, M.D. Vilisova, I.A. Prudaev. *Semiconductor devices based on gallium arsenide with deep impurity centers*. Publishing House TSU, Tomsk (2016). 256 p. (in Russian).
- [5] N.G. Filonov, I.V. Ivonin. *Electrophysical properties of structures with a Schottky barrier based on gallium arsenide*. Izd.dom TGU, Tomsk (2018). 364 p. (in Russian).
- [6] *Crystal Growth Technology* / Eds H.J. Scheel, T. Fukuda. John Wiley & Sons Ltd., Chichester, UK (2003). 668 p.
- [7] G.E. Tsyrlin, V.G. Dubrovsky, N.V. Sibirev, I.P. Soshnikov, Yu.B. Samsonenko, A.A. Tonkikh, V.M. Ustinov. *FTP* **39**, 5, 587 (2005). (in Russian).
- [8] P.A. Alekseev, M.S. Dunaevsky, A.O. Mikhailov, S.P. Lebedev, A.A. Lebedev, I.V. Ilkiv, A.I. Ridges, A.D. Buravlev, G.E. Tsyrlin. *FTP* **52**, 12, 1507 (2018). (in Russian).
- [9] M.G. Krzhizhanovskaya, V.A. Firsova, R.S. Bubnova. *Primenenie metoda Rietvelda dlya resheniya zadach poroshkovoy diffraktometrii* (Application of the Rietveld method for solving problems of powder diffraction). Izd-vo SPbGU, SPb (2016). 68 p. (in Russian).
- [10] Tsubota M., Kitagawa J. *Sci. Rep.* **7**, 1, 15381 (2017).
- [11] G.S. Pawley. *J. Appl. Cryst.* **14**, 6, 357 (1981).
- [12] A. Le Bail. *Powder Diffraction* **20**, 4, 316 (2005).
- [13] *Handbook on Big Data and Machine Learning in the Physical Sciences* /Eds K.K. van Dam, K.G. Yager, S.I. Campbell, R. Farnsworth, M. van Dam. *Advanced Analysis Solutions for Leading Experimental Techniques*. World Scientific Publishing Co, N.J. (2020). V. 2. 1000 p.
- [14] *International Tables for Crystallography* / Eds C.J. Gilmore, J.A. Kaduk, H. Schenk. Wiley (2019). V. H: Powder Diffraction. 932 p.
- [15] A. Tlahuice-Flores. *Phys. Chem. Chem. Phys.* **17**, 8, 5551 (2015).
- [16] M. Suleiman, C. Borchers, M. Guerdane, N.M. Jisrawi, D. Fritsch, R. Kirchheim, A. Pundt. *Z. Phys. Chem.* **223**, 1–2, 169 (2009).
- [17] P. Andrezza, C. Mottet, C. Andrezza-Vignolle, J. Penuelas, H.C.N. Tolentino, M. De Santis, R. Felici, N. Bouet. *PRB* **82**, 15, 155453 (2010).
- [18] A. Leonardi, P. Scardi. *Metal. Mater. Trans. A* **47**, 12, 5722 (2016).
- [19] S. Plimpton. *J. Comp. Phys.* **117**, 1, 1 (1995).
- [20] Sandia Corporation. LAMMPS User Manual. Sandia National Laboratories, Albuquerque, NM / Livermore, CA (2003).
- [21] B.F. Ormont. *Introduction to physical chemistry and crystal chemistry of semiconductors*. Vyssh. shk., M. (1982). 528 p. (in Russian).
- [22] M.E. Boyko, M.D. Sharkov, A.M. Boyko, A.V. Bobyl, S.G. Konnikov, N.S. Budkina. *ZhTF* **85**, 11, 1 (2015). (in Russian)
- [23] W.H. Zachariasen. *Theory of X-Ray Diffraction in Crystals*. Dover Publications, NYC (1967). 256 p.
- [24] *International Tables for Crystallography* / Ed. E. Prince. Kluwer Academic Publishers, Dordrecht, Boston London (2004). V. C: Mathematical Physical and Chemical Tables. 1000 p.
- [25] A.V. Saveliev. *General physics course. V. 2. Elektrichestvo i magnetizm, volny, optika*. Nauka, M. (1988). 496 p. (in Russian).